

High-speed multiple window readout of Hawaii-1RG detector for a radial velocity experiment

Nagaraja Bezawada* and Derek Ives

UK Astronomy Technology Centre, Royal Observatory, Blackford Hill, Edinburgh EH9 3HJ, UK

ABSTARCT

The next generation of Radial Velocity Spectrometers for 8 metre class telescopes will require very high resolution spectroscopy in the near infrared 1 – 2.5 μ m regime. One of the main engineering goals for such an instrument design is to readout at high speed, multiple windows, which are concurrently imaging bright reference arc lines whilst also integrating very faint source spectra on the rest of the detector. The Hawaii-1RG/2RG readout multiplexers offer a programmable window readout mode which allows non-destructive readout of multiple regions which are programmable in any size and location on the array. We present results from the characterisation of an engineering grade HIRG detector using an SDSU III controller and the effects of the multiple window readout, if any, on the noise and cross-talk performance of the rest of the detector. The detector performance results will also include quantum efficiency measurements in J, H and K pass bands, dark generation, noise, full well, linearity, inter-pixel capacitance and persistence.

Keywords: Hawaii1RG, IR Detector, SWIR, Window Readout

1. INTRODUCTION

The next generation of Radial Velocity Spectrometer instruments will require a shortwave infrared (SWIR) detector array of ~4K x 4K format in order to acquire sufficient M dwarf star absorption features with a resolution of approximately 1m/s. The simultaneous arc-line calibration method requires accessing pre-determined selectable multiple windows which are imaging bright reference arc-lines whilst the rest of the detector array integrates the faint object absorption features. With the present generation of near infrared detectors, this can be achieved with a close mosaic of 4 of the 2K x 2K SWIR Hawaii-2RG detectors.

The Hawaii-1RG/2RG readout integrated circuits (ROIC or multiplexer) offer various features such as selectable outputs, low/ high speed operating modes, simultaneous window access, various reset modes and a variety of clocking modes etc. The multiplexer allows the programming of any desired location and size of window which can then be independently reset or read. This allows implementation of guide star observations on a sub-window whilst integrating the science observations on the rest of the detector. Several such windows can be accessed in sequence by programming the multiplexer for one window operation at a time. This feature allows the user to define a number of small windows around the bright reference spectral lines across the detector and then being able to read or reset these to avoid saturation of these lines whilst integrating the object spectra on the rest of the detector. The multiplexer can be configured to provide the window data on a separate output or through one of the standard outputs that are used to read the full frame.

At high precession, the sensitivity of the spectrometer depends largely on the performance of the detectors at the instrument background level as the sky background is negligible. The key performance parameters such as quantum efficiency, dark generation, readout noise, temporal stability, charge diffusion, persistence all affect the sensitivity of the instrument. In this paper we present the details of the operation of a Hawaii-1RG (engineering grade) detector and the implementation of the multiple window readouts along with other results from the device characterisation such as the inter-pixel capacitance, charge diffusion due to inter-pixel capacitance, quantum efficiency, linearity, full well, dark generation, temporal stability, persistence and cross-talk. The inter-pixel capacitance is estimated using a stochastic method. The point spread function generated by the inter-pixel coupling capacitance is also obtained by defining a single pixel window that is kept under reset whilst integrating the charge in the neighboring pixels. The symmetry in the spread

* e-mail: nnb@roe.ac.uk

of the charge from neighboring pixels is also investigated as is the change, if any, of the PSF across the detector due to inter-pixel capacitance.

2. TEST SETUP

A suitable detector mount for the Hawaii-1RG detector was developed (Figure 1) to use with our existing test cryostat, with minimal modifications. The detector is mounted on a molybdenum base plate using 4 Cu/W studs and molybdenum spacers. The mount plate is then attached to a thermally controlled stage ensuring good thermal contact with the detector mount plate. The detector is cooled symmetrically through 4 mounting studs and one of the mounting positions is strain relieved by two splits in the mounting plate. The base plate, on which the assembly is mounted, is thermally stabilized to <10mK by a Lakeshore temperature controller.

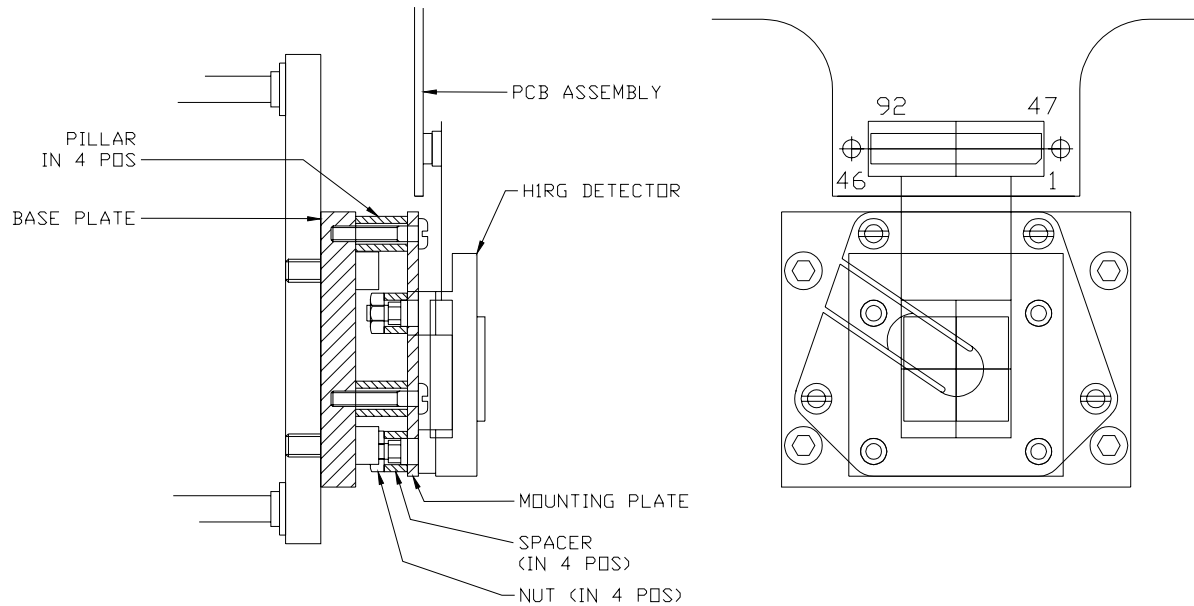


Figure 1: Hawaii-1RG detector mount design

A cryogenic preamplifier board, that interfaces to the detector flex connector, provides two preamplifiers, bias decoupling and over-voltage protection on all the bias and clock lines. The detector flex provided by Rockwell provides an interface to the pin grid array behind the detector through a 92-pin Hirose high density connector. The preamplifier is a differential amplifier design using CMOS TLC2274 op-amps which work reliably at cryogenic temperatures. The reference input to the differential preamplifier is derived from either the internal detector reference output or from an external controller reference voltage. The test setup showing the detector in its mount and the preamplifier board in the cryostat is shown in Figure 2.

The cryostat also consists of a manually selectable filter wheel that mounts directly above the detector on the pillars seen in Figure 2. The light path from the cryostat window to the filter wheel and then on to the detector is surrounded by a cold, low background baffle, ensuring that the detector doesn't see directly any warm surfaces within the cryostat. The Generation-3 AstroCam (SDSU) controller based on in-house developed data acquisition software is used to control and readout the detector.

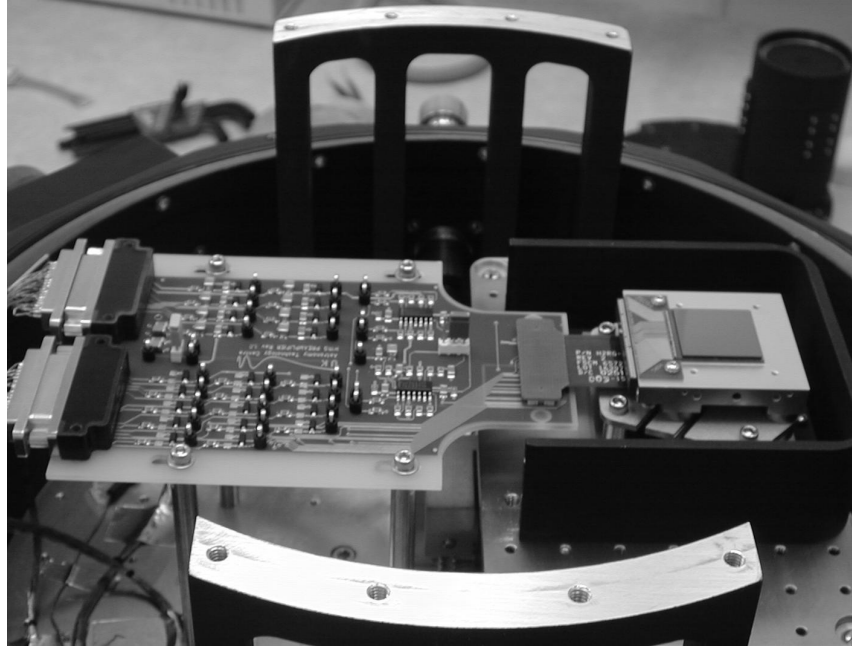


Figure 2: Detector in its mount and the pre-amp PCB in the test cryostat

3. DETECTOR OPERATION

The Hawaii-1RG detector is operated at 72K and is read out using only two outputs. A separate output for the window output and the reference output are also used. The reference output is connected to the reference input of the differential preamplifier providing some automatic compensation for any minor thermal drifts. The detector is operated at 100 kHz pixel rate on each channel allowing a full frame readout in ~ 5.4 s using the on-chip source followers. A 10k ohm load resistor is used to pull the source of the output source follower to the VDDA bias supply and the detector is reverse biased to 0.5V ($V_{\text{reset}} = 0.0$, $V_{\text{Dsub}}=0.5$). The various registers and the operation of the detector are programmed using a set of dedicated serial lines (CSB, DATACLK and DATAIN). In order to use these dedicated serial lines, the detector first needs to be programmed to select the dedicated serial interface using the horizontal clock lines (HCLK and LSYNC) along with the CSB line.

After powering up the array, the ROIC needs a reset which sets all the internal registers to their default states. Subsequently, all the required registers are programmed (e.g. selecting the on-chip output buffers, speed of operation, number of outputs, etc) with the appropriate 12 bit words. The ROIC is designed to prevent single event upset (SEP) by providing shielding of the multiplexer programmable registers. The SEP guard is further protected by the main reset, in that once the registers are programmed, they cannot be re-programmed unless a main reset is issued. The window mode can be enabled by the corresponding bits (VWMEN and HWMEN) in the 'MiscReg' register or by the external VERTWMEN and HORIWMEN lines. In this application, as we intended to access several windows in sequence, we have used the VWMEN and HWMEN bits in the 'MiscReg' to switch between window and full frame mode. This requires programming the new window co-ordinates in the corresponding start / stop window registers and enabling the window mode using the 'MisCReg' register every time the mode is changed.

The detector is kept continuously under reset when idling. The reset anomaly seen in Hawaii2 detectors is also seen in this detector. A simple CDS frame shows a gradient which can be reduced by doing a couple of fast dummy reads before taking the first frame of the CDS sequence. It is noticed that when the fast 'Row Reset' is used to reset the array before taking the first frame in a CDS sequence, that the difference frame of two subsequent CDS frames is not flat and a small gradient is still present. The difference frame is much flatter when the array is reset using row reset as before but at the same time addressing every pixel in the row being reset as done in the case of read frame.

3.1 Window mode operation

The window mode is enabled by the corresponding bits (VWMEN and HWMEN) in the registers. Once the window coordinates are programmed and the window mode is enabled, the window data can be immediately accessed. The programming involves resetting the internal registers (main reset) and programming the start and stop registers for the vertical and the horizontal window scan registers. The window mode can then be enabled by the corresponding bits in the MisReg or using the external lines. The window data can either be routed through normal output#7 or through the separate window output.

The window size can be any size in a rectangular format within the allowed pixel format. A single pixel window can also be defined. Using a single pixel window, it is possible to reset this pixel continuously whilst its surrounding neighbours integrate the signal. This method allows the estimation of the charge diffusion into the pixel that is under reset from its neighbouring pixels caused by the inter-pixel capacitance. This method has been described previously by Finger, et al¹. We have extended this method to measure the inter-pixel capacitance for all pixels along any row or column as described below.

3.2 Measurement of inter pixel capacitance along any line or column

A model developed at the UKATC on the effect of the inter-pixel capacitance on the radial velocity sensitivity² shows that whilst symmetrical charge coupling to neighbouring row/ columns does not induce any velocity shifts, the variation in charge coupling can cause variation in the velocity error. To measure the capacitive coupling across the detector, the window feature was used to define a window of one full row or one column to investigate the extent and the variation of the interpixel capacitive coupling. A few rows and columns across the array are kept under reset whilst integrating the remaining pixels. This allowed us to measure, from a normalized difference frame, the extent and the scatter of the capacitive coupling in a row or column and its symmetry from its neighbouring rows or columns. The scatter is estimated to be around 0.1 – 0.15% of the values of the mean of the capacitive coupling as shown in the Figure 3a and the scatter in the coupling across a row and a column is shown in Figure 3b. Both columns and rows showed symmetric capacitive coupling across the array.

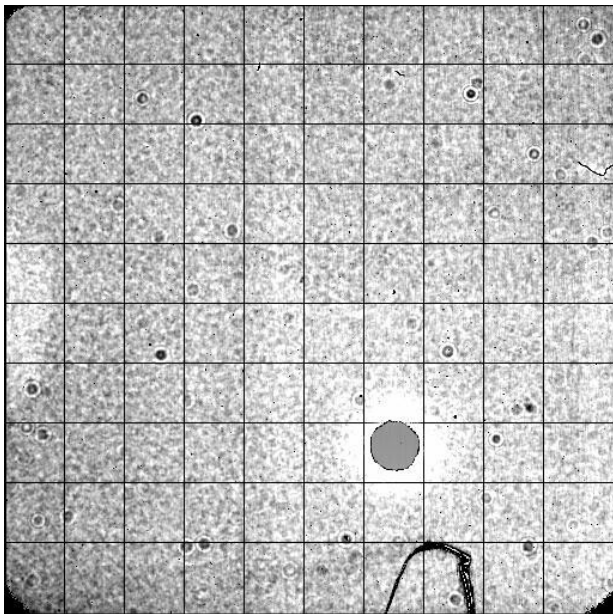


Figure 3a: Several rows and columns under reset. Charge coupling is symmetric across the array.

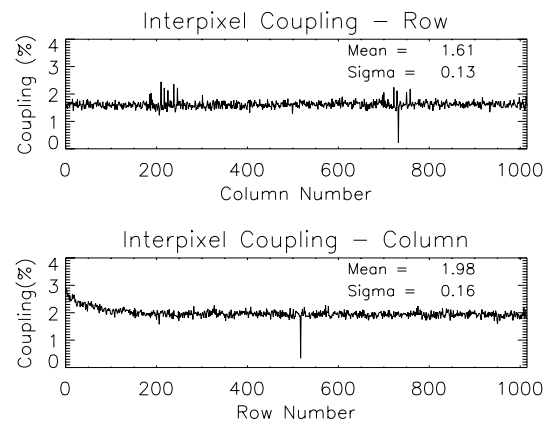


Figure 3b: Scatter in the charge diffusion across a row (above) and a column (below)

3.3 Multiple window mode operation

Programming for multiple windows is no different to a single window programming. Several windows can be programmed consecutively in sequence to allow a read or reset operation on one window at a time. It is required to re-program all the internal registers (including registers for selecting number of outputs, speed of operation, selecting buffers etc) when programming the new window co-ordinates in the window start/stop registers. In our setup, up to 32 windows are defined and readout in sequence as shown in Figure 4. In this example, the windows are positioned to map out the word "ATC" on the array. At 100 kHz speed of operation, it takes approximately 4.4ms for programming and reading of a 20 x 20 window, of which, in our SDSU controller setup, it requires approximately 100 μ s overhead for window programming. For 32 windows we can run at a windowed read rate of approximately 7 Hz.

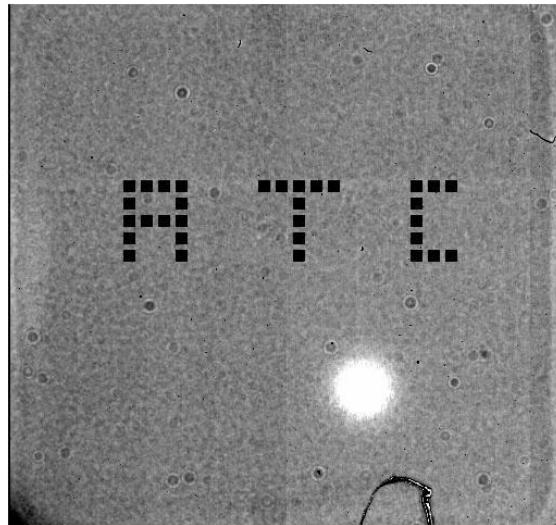


Figure 4: Multiple windows under reset whilst the rest of the frame integrating signal

4. DETECTOR PERFORMANCE

4.1 Conversion gain

The system gain is estimated from photon transfer (histogram method based on signal mean-variance) using several pairs of identical flats. Identical pairs of flats were obtained by varying the detector integration time whilst the temperature of the blackbody source is kept constant. Signal saturation is obtained from the noise rollover point in the mean signal – variance plot (Figure 5a). Figure 5b shows non-linearity measured from 20 – 80% of the full well.

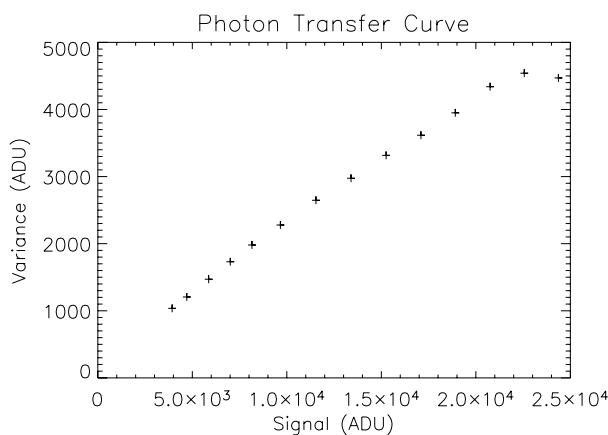


Figure 5a: Full well measured from noise rollover

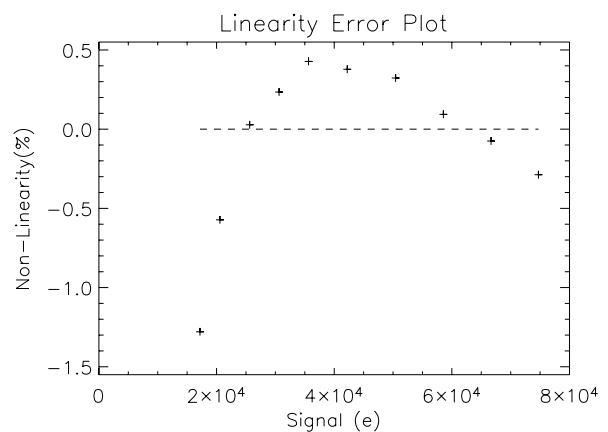


Figure 5b: Non-linearity (~1.7% from 20 to 80% full well)

System gain is measured from a small box (25 x 25 pixels) positioned all over the detector and from the pairs of flats corresponding to 20 – 50% of full well. This is shown in the Figure 6a. The mean of the histogram is taken as the system gain and is used (after correcting for inter-pixel capacitance – see section 4.2) for all subsequent measurements. System gain is also measured using a temporal method from a stack of 200 CDS frames in which a mean and variance is estimated for every pixel. Figure 6b shows the gain histogram for the entire frame. The mean and the median of the histogram in Figure 6b agree very closely to the mean of the histogram obtained from the spatial (moving box) method. As the conversion gain changes with the signal level due to the capacitance change of the reverse biased diodes, both these measurements are obtained at approximately the same signal level for comparison. We find that the conversion gain (and hence the transimpedance conversion gain) changes by ~15% for 20 – 70% of full well. The transimpedance conversion gain is measured to be $4.1\mu\text{V}/e^-$ at 30% of full well.

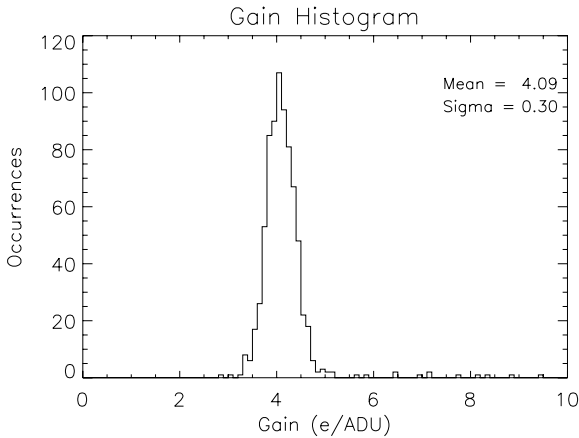


Figure 6a: System gain measured from spatial method

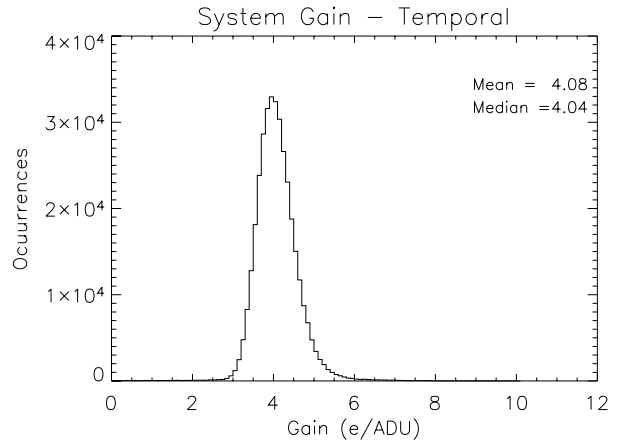


Figure 6b: System gain measured from temporal method

4.2 Node capacitance

In order to estimate the pixel node capacitance, the source follower gain has to be calculated first. The source follower gain is measured by keeping the detector under continuous reset (reset enabled high during read or reset, and the detector is zero biased). The shift in the output DC level corresponding to the change in the V_{reset} enables the measurement of the combined source follower gain (pixel unit cell source follower gain x output source follower gain). Figure 7a shows the histogram of the source follower gain for the frame. The mean source follower gain is ~0.92 and is used to estimate the nodal capacitance which is estimated to be approximately 36fF using the value for transimpedance obtained from the photon transfer method.

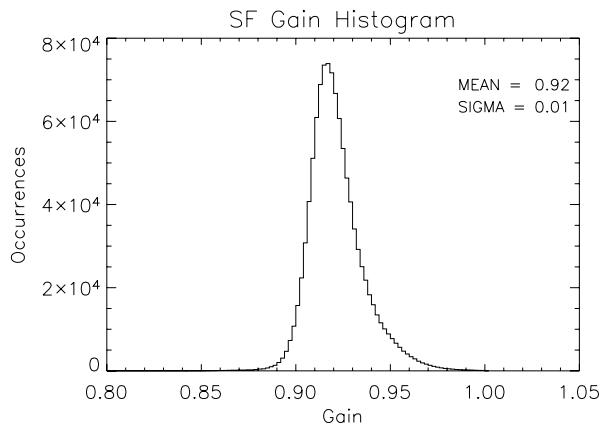


Figure 7a: Source follower gain for the HIRG detector

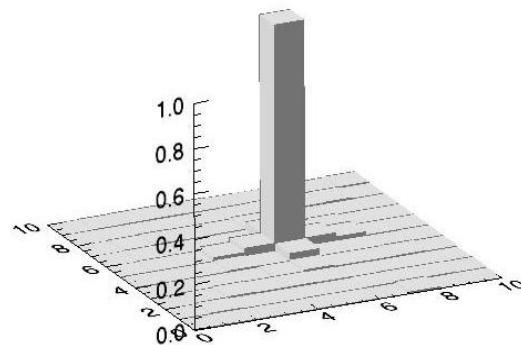


Figure 7b: Surface plot of inter-pixel capacitance using 2D auto correlation method

It has been shown that the inter-pixel capacitance in these hybrid detectors dampens the shot noise causing the over-estimation of the nodal capacitance from the photon transfer method^{3,4}. A stochastic method based on a 2-dimensional auto correlation function is used to estimate the noise correlation damping factor due to the inter-pixel capacitance and is found to be approximately 1.15 (for 5 x 5 pixels). A normalized surface plot of the pixel coupling is shown in Figure 7b. The actual nodal capacitance after correcting for the inter-pixel capacitance is approximately 30.6fF.

4.3 Quantum efficiency

The quantum efficiency of the detector is measured in astronomical Y, J, H and K bands using blackbody radiometry. It is to be noted that the uncertainty in these measurements is up to ~12% and is mainly due to the blackbody temperature inaccuracy, its surface emissivity and the temperature dependence of the filter pass-band transmission. Figure 8 shows the QE histogram for the H band. The detector shows a skew of almost a factor of two in the responsivity from short wavelength to longer wavelength as shown in the Table 1.

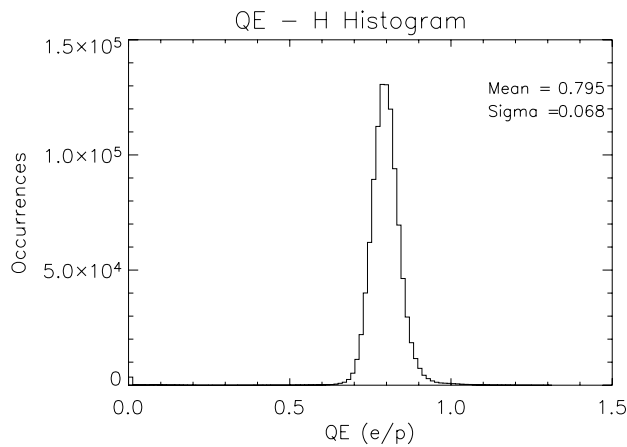


Table 1: Quantum efficiencies measured in Y, J, H and K bands on the engineering Hawaii-1RG detector

Pass band	QE (%)
Y(1.01 – 1.07)*	51.7
J (1.18 – 1.34)	56.4
H (1.49 – 1.79)	79.5
K (2.10 – 2.41)	95.4

* - Bandwidth is reduced due to additional shortwave pass band filter used to reject red-leaks.

Figure 8: QE histogram in H-band

4.4 Read noise

The read noise is measured using both the pixel-to-pixel and temporal methods. The pixel-to-pixel method is the simplest method for calculating the read noise and is derived from two identical CDS dark frames. The two identical frames are subtracted one from another and the resultant frame is divided by $\sqrt{2}$ to account for the noise increase due to subtraction. The standard deviation for a small box (25 x 25 pixels) multiplied by the system gain (e/ADU) gives the result in electrons for the pixel-to-pixel noise in that box region. Many such noise values are obtained by moving the box all over the frame, whilst values three-sigma from the mean are excluded from this measurement of the read noise. The mean value of the read noise calculated using this method is approximately $26e^-$ (rms). The temporal method involves estimating noise for every pixel from a stack of CDS frames. In our case, a stack of 20 CDS frames were used to generate a noise frame. The histogram of the temporal noise frame is shown in Figure 9a. The temporal method gave a noise measurement of $22e^-$ (rms). Both of these methods resulted in slightly higher read noise than is expected for these detectors. It is to be noted that this detector is an engineering grade device and hence it may be reasonable to expect the higher read noise. The read noise for multiple non-destructive reads reduces to $\sim 7e^-$ (rms) with 128 non destructive readout frames and bottomed out there after as shown in Figure 9b.

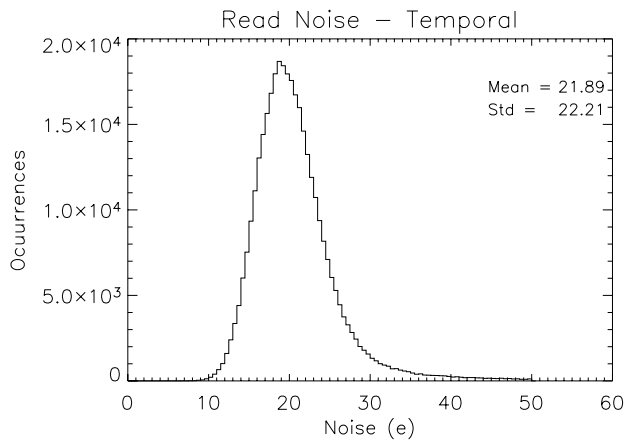


Figure 9a: CDS Read noise (temporal method)

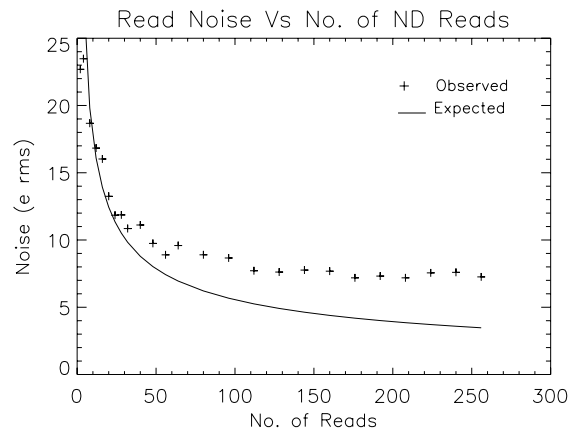


Figure 9b: Read noise with multiple ND frames

4.5 Dark generation

The detector showed a large gradient (reset anomaly) in a simple CDS frame following the detector reset. The gradient is reduced by performing a couple of fast reads as was done with the Hawaii-2 detectors of the WFCAM⁵. The frames showed large counts in a CDS frame even with minimum detector integration time, but two similar CDS frames are identical and any profiles subtract out flat. These counts in a CDS frame reduce with time following the reset and it takes about couple of hours to settle to the final value. Figure 10a shows the rate of apparent dark generation (note the transient is not true dark current as explained below) obtained from a series of non-destructive read frames every 30s following the detector reset. The dark generation sufficiently away from the dark transient represents the true dark generation and is $\sim 0.4 \text{ e}^-/\text{s}/\text{pixel}$. The histogram of the dark generation from a small region is shown in Figure 10b. It is to be noted that the test setup is not optimized for very low background tests.

The dark transient appears to have no significant dark component in it. Two sets of identical frames are obtained along the dark transient following the detector reset. The read noise estimated from the two similar frames from these two sets showed no increase in the read noise as shown in the Figure 11 suggesting there is no real dark component in the dark transient. The apparent high dark generation is probably due to change in the pixel DC level to its settling value following the reset.

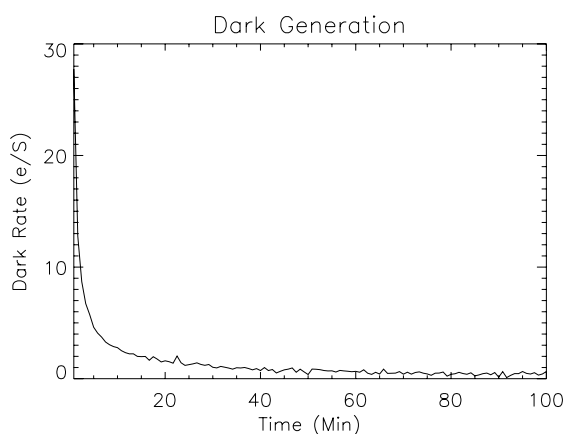


Figure 10a: Apparent dark generation transient following the detector reset

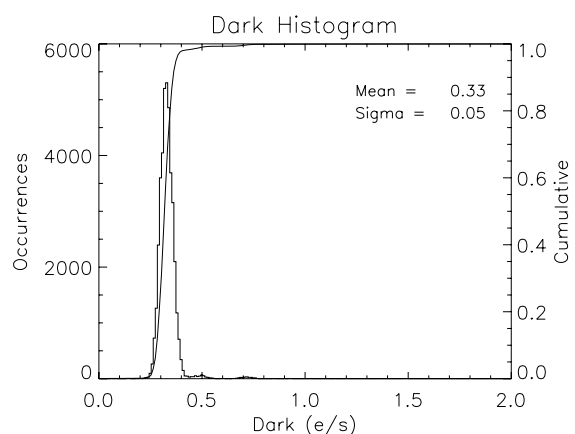


Figure 10b: Dark generation histogram from a 200 x 200 region

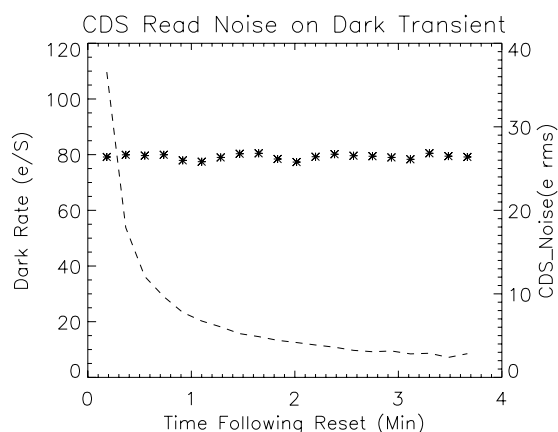


Figure 11: Read noise along the dark transient. The dark transient has no noise associated with it.

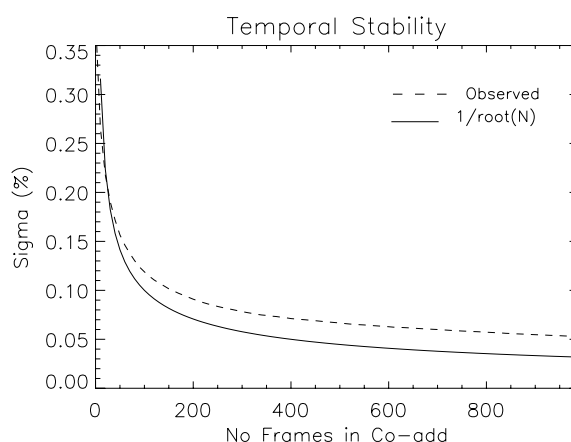


Figure 12: Temporal stability from number of co-adds

4.6 Temporal stability

In order to investigate the flat-field stability of the detector, co-adds of many identical flats are used to improve the flat-field accuracy. A window of 200 x 200 pixels is used and a sequence of 2000 CDS frames are obtained, each flat field having $\sim 15k e^-$ signal from a K band setup. A first set of several co-adds from different numbers of frames (e.g. using the first 10 frames, first 20 frames, all the way up to using the 1000 frames) are obtained from the first 1000 frames. Similarly a second set of co-adds are created from the later 1000 CDS frames. The time difference between the start of each 1000 frame set is approximately three hours. Every co-added frame in the first set is divided by the corresponding co-added frame in the second set and the standard deviation in the resultant frame is plotted against the number of frames in a given co-add as shown in Figure 12. For a comparison, $1/\sqrt{n}$ (n being the number of frames in a given co-add) is also plotted in the same graph. As can be seen from the plot, the flat-field stability is $\sim 0.05\%$ for co-adds of $\sim 15 \times 10^6 e^-$ of signal. The wavelength dependency of the temporal stability is still to be investigated.

4.7 Persistence

Persistence signal is investigated by exposing the detector to different saturation levels by varying the flux whilst keeping the exposure time constant. The persistence signal is measured in 15s follow on images where a cold blank has been positioned in front of the detector. It is to be noted that the amount of persistence signal is proportional to the integration time of the latency image. It appears that there is no significant increase in the persistence signal with the signal level until just about the saturation point of the detector is reached. Figure 13 shows the decay of the persistence signal current measured from the 15s dark integrations following the exposure to various fluence levels.

4.7.1 Persistence due to over saturation

Persistence signal seems to take several hours or even days to decay down if the detector has been heavily oversaturated. During the acquisition of the window data for the temporal stability measurement, the detector is continuously exposed to the radiation. Only a windowed region is reset and read continuously whilst nothing has been done to the remaining pixels of the detector. These remaining detector pixels will have been integrating signal and eventually over-saturated. At the end of the data acquisition, the cold blank is positioned in front of the detector, and the detector is switched into the full frame mode of operation and left to perform continuous resets for a few hours. A dark frame for 1 hour integration (Figure 14) shows the effect of the over-saturation. The dark generation in the rest of the frame is approximately two times higher than the dark generation in the window region which was not saturated. This higher dark generation in the rest of the frame could be seen even after several hours ($\sim 4\%$ level after ~ 8 hours). Traces of the window region could be seen even after completely de-powering and then re-powering of the detector.

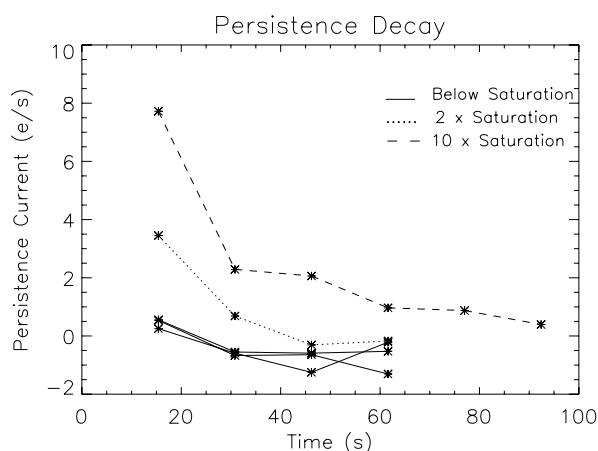


Figure 13: Persistence signal decay

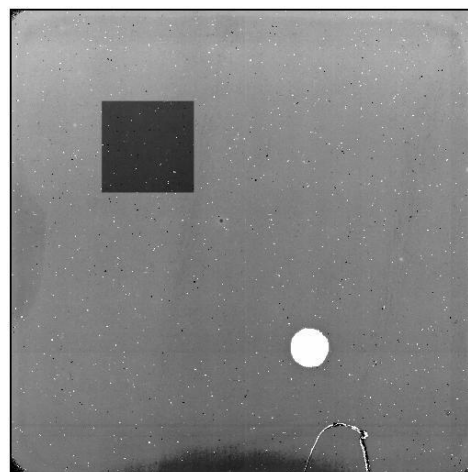


Figure 14: Dark generation (1hr) bitmap showing higher dark generation in the frame other than the window region.

4.8 Cross talk

In our setup, the detector is read through two outputs each handling 512 columns x 1024 rows. A small blackbody aperture was imaged onto one side of the detector which read through channel 1. The signal in the channel 2 was then investigated for the resulting electrical cross-talk. As shown in the Table 2, the cross-talk in the channel 2 is proportional to the signal in the channel 1. The cross-talk of the 8 channel controller video boards was measured to be ~0.002% between neighbouring channels. We therefore surmise that the measured crosstalk is a function of the detector itself or the common biases to the detector outputs. Efforts will be made to isolate the source of this cross-talk, for example, by providing separate low impedance output source bias supplies for the two outputs.

Table 2: Electrical cross-talk between the two readout channels

Signal level in Channel-1	Cross-talk in Channel-2 (%)
Full well	0.18
$\frac{3}{4}$ Full well	0.18
$\frac{1}{2}$ Full well	0.14
$\frac{1}{4}$ Full well	0.08

4.9 Effect of window reset

Resetting a window causes a slight shift in the pixel DC values along the same rows and to all pixels either side of the window. Figure 15a shows a CDS dark frame with minimum detector integration time. The array is reset and the first frame is read out. The three windows are then accessed sequentially and reset before the second full frame is readout. The CDS frame shows a slight increase in the pixel DC values (bands) along the rows corresponding to the window regions. This effect can be eliminated when a similar window reset is also performed before the first full frame readout. The effect is not seen in the Figure 15b in which the window resets are performed before the first and the second full frame readouts of the CDS frame. It is observed only the reset causes this effect. Accessing the windows for reads doesn't show this effect. So long as the windows are reset just before the first full frame, the windows can be accessed several times for read or reset operation before the second full frame without having the bands in the CDS frame.

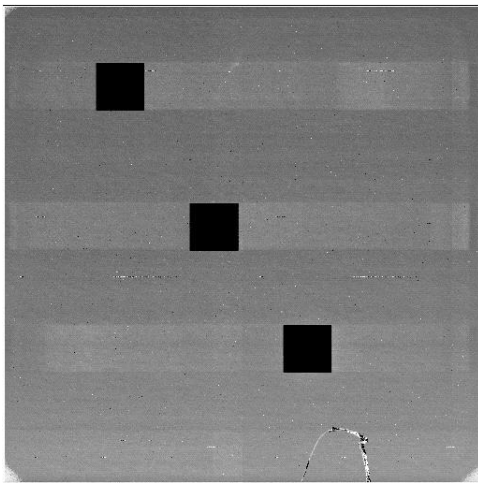


Figure 15a: Window resetting causes a small change (~ 15 ADUs) in the DC levels of all the pixels in the entire row. Window is reset before the 2nd frame in a dark CDS frame

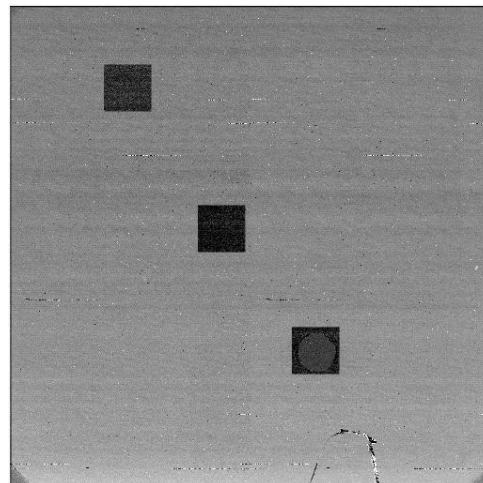


Figure 15b: The effect is eliminated by taking identical window resets before the 1st CDS frame

5. CONCLUSION

An engineering grade Hawaii-1RG detector has been tested in an existing test setup with a suitable modification to the detector mount. The detector is operated at 72K in slow speed through two outputs along with a separate output for the window mode. The window feature of the detector is used to define a single pixel window to investigate the point spread function generated by the inter-pixel capacitance. Single line and column windows are defined in order to estimate the variance in the capacitive coupling. The scatter in the capacitive coupling is of the order 0.1 – 0.15 of the value coupling along a column or row. A 2D auto-correlation function is used to estimate the inter-pixel capacitance in the detector. A correlation factor 1.15 has been obtained and is used to correct the conversion gain obtained from the photon-transfer method. The average pixel nodal capacitance is estimated to be ~ 30 fF. The detector has been successfully operated in multiple window readout mode and it is found that there is no added noise in the rest of the frame due to window operation. There are also no significant over-heads in the programming for windows. The performance parameters of the detector such as quantum efficiency, dark generation, read noise are reported. It is found that the apparent high dark generation following the reset has no true dark component associated with it. This detector showed a skewed responsivity from short to longer wavelengths. The persistence signal is roughly constant until saturation, but then increases rapidly with hard saturation. When the detector is over-saturated, it takes several hours for the persistence signal to decay down and resetting or de-powering the array has a negligible effect on it. The electrical cross-talk between the readout channels needs further tests to reduce the coupling. Flat-field stability $\sim 0.05\%$ (through K band) could be achieved by co-adding several hundred flats.

6. ACKNOWLEDGEMENTS

We would like to express our sincere thanks to Rockwell Scientific for the long term loan of the detector and useful discussions. Thanks are also due to Gert Finger at ESO for useful suggestions on the operation of the detector. At the UKATC we would like to thank Adrian Webster for the modeling of the detector cross-talk and discussions and Tom Paul for the design of the detector mount in the test cryostat.

REFERENCES

1. G. Finger, J. Garnett, N. Bezawada, R. Dorn, L. Mehrgan, M. Meyer, A. Moorwood, J. Stegmeir, G. Woodhouse, Nuclear Instruments and Methods in Physics Research A, In press.
2. A. Webster, Internal document, 'The effect of detector cross-talk on the radial-velocity sensitivity' Mar 2006

3. G. Finger, J. W. Beletic, R. Dorn, M. Meyer, L. Mehrgan, A. F. M. Moorwood, J. Stegmeier, Conversion gain and inter-pixel capacitance of CMOS hybrid focal plane arrays, *Scientific Detectors for Astronomy 2005*, p. 477 – 490
4. A. C. Moore, Z. Nincov, W. J. Forrest, Interpixel capacitance in non-destructive readout focal plane arrays, *Proc. SPIE 5167*, p.204-215
5. D. Ives, The UKIRT Wide Field Camera, *Scientific Detectors for Astronomy 2005*, p.81 – 86